The Astrophysical Journal, 803:20 (15pp), 2015 April 10 doi:10.1088/0004-637X/803/1/20

THE CHANGING FRACTIONS OF TYPE IA SUPERNOVA NUV–OPTICAL SUBCLASSES WITH REDSHIFT

Peter A. Milne[1], Ryan J. Foley[2,3], Peter J. Brown[4], and Gautham Narayan[5]
[1] University of Arizona, Steward Observatory, 933 N. Cherry Ave., Tucson, AZ 85719, USA; pmilne@as.arizona.edu
[2] Astronomy Department, University of Illinois at Urbana-Champaign, 1002 West Green Street, Urbana, IL 61801, USA; rfoley@illinois.edu
[3] Department of Physics, University of Illinois Urbana-Champaign, 1110 West Green Street, Urbana, IL 61801, USA
[4] George P. and Cynthia Woods Mitchell Institute for Fundamental Physics & Astronomy, Texas A. & M. University, Department of Physics and Astronomy, 4242 TAMU, College Station, TX 77843, USA; pbrown@physics.tamu.edu
[5] National Optical Astronomy Observatory, P.O. Box 26732, Tucson, AZ 85726, USA; gnarayan@noao.edu
Received 2013 November 26; accepted 2015 February 8; published 2015 April 9

ABSTRACT

Ultraviolet (UV) and optical photometry of Type Ia supernovae (SNe Ia) at low redshift have revealed the existence of two distinct color groups, composed of NUV-red and NUV-blue events. The color curves differ primarily by an offset, with the NUV-blue $u - v$ color curves bluer than the NUV-red curves by 0.4 mag. For a sample of 23 low-redshift SNe Ia observed with *Swift*, the NUV-red group dominates by a ratio of 2:1. We compare rest-frame UV/optical spectrophotometry of intermediate- and high-redshift SNe Ia with UVOT photometry and *Hubble Space Telescope* spectrophotometry of low-redshift SNe Ia, finding that the same two color groups exist at higher redshift, but with the NUV-blue events as the dominant group. Within each red/blue group, we do not detect any offset in color for different redshifts, providing insight into how SN Ia UV emission evolves with redshift. Through spectral comparisons of SNe Ia with similar peak width and phase, we explore the wavelength range that produces the UV/optical color differences. We show that the ejecta velocity of NUV-red supernovae (SNe) is larger than that of NUV-blue objects by roughly 12% on average. This velocity difference can explain some of the UV/optical color difference, but differences in the strengths of spectral features seen in mean spectra require additional explanation. Because of the slightly different $b - v$ colors for these groups, *NUV-red SNe will have their extinction underestimated using common techniques*. This, in turn, leads to underestimation of the optical luminosity of the NUV-blue SNe Ia, in particular, for the high-redshift cosmological sample. Not accounting for this effect should thus produce a distance bias that increases with redshift and could significantly bias measurements of cosmological parameters.

Key words: supernovae: general

1. INTRODUCTION

Type Ia supernovae (SNe Ia) are very luminous, with a well-understood variation of their peak optical luminosities as a function of their light-curve shapes, the width–luminosity relation (WLR; $\Delta m_{15}(B)$: Phillips 1993; Δ: Riess et al. 1996; Jha et al. 2006a; stretch(s): Perlmutter et al. 1997; SiFTO: Conley et al. 2008). The empirically derived width–luminosity relation has allowed SNe Ia to be utilized to study the expansion of the universe, revealing that the expansion is currently experiencing a period of acceleration (Riess et al. 1998; Perlmutter et al. 1999). In order to lower the scatter in distance determinations, the larger sample of all SNe Ia is reduced to a group of so-called "normal" SNe Ia, a group that follows a regular variation of their properties with the width of the peak of their optical light curves (i.e., scaling). The reduced sample eliminates narrow-peaked SNe Ia (see Taubenberger et al. 2008; Krisciunas et al. 2009), SNe Iax (Li et al. 2003; Foley et al. 2013), candidates for super-Chandrasekhar SNe Ia (e.g., Howell et al. 2006; Scalzo et al. 2010) and individually anomalous events (e.g., Li et al. 2001; Foley et al. 2010; Maguire et al. 2010; Sullivan et al. 2011). The reduced sample comprises roughly half of the SNe Ia discovered, and will be the focus of this work.

A key element of the cosmological utilization of SNe Ia is the assumption that the SN Ia phenomenon does not change as the universe aged, or that any changes continue to follow the empirical laws derived for nearby normal SNe Ia. For example, the method can work if higher-z SNe Ia tend to have broader optical light curves, as long as the luminosities of those supernovae (SNe) still follow the WLR for that peak width. A problem would arise if higher-z SNe Ia had brighter or fainter luminosities for the same light-curve shape. An example of one such problem was reported by Sullivan et al. (2010), who claim a dependence of SN Ia luminosity on the mass and specfic star formation rates of the host galaxy. As these characteristics vary with redshift, a systematic error is introduced to cosmological analyses at the 0.08 mag level.

Spectral modeling makes it clear that iron-peak elements significantly impact the ultraviolet (UV) spectral-energy distribution (SED) of SNe Ia (e.g., Kirshner et al. 1993; Hőflich et al. 1998; Lentz et al. 2000; Sauer et al. 2008; Hachinger et al. 2013; Mazzali 2013). Theoretical models of a thermonuclear explosion of an SN Ia have explored the effects of varying the progenitor metallicity or explosion physics on the resulting ^{56}Ni production and distribution, as well as on the expansion velocities (Hőflich et al. 1998; Lentz et al. 2000; Timmes et al. 2003; Sauer et al. 2008; Walker et al. 2012). All simulations suggest that the UV emission is much more strongly affected by metallicity variations than the optical emission, and would lead to variations in the UV-optical colors of SNe Ia with different progenitor metallicities. Since the progenitor metallicity is one aspect of an SN Ia explosion that would be expected to change with redshift, it is vital to establish the nature of the progenitor metallicity–UV SED correlation. However, there is not a consensus about the magnitude of that correlation, underscoring how challenging it is to model a complete time-evolving spectrum of an SN Ia.

Further, as there are multiple classes of progenitor systems suggested (e.g., single versus double degenerate), as well as multiple explosion scenarios (e.g., delayed detonations versus deflagrations versus double detonations), it is not clear that progenitor metallicity differences will be the dominant factor in variations of the UV-optical SED (Roepke et al. 2012; Foley et al. 2012b). With all the challenges facing theoretical modeling, observational efforts to characterize the time evolution of the UV-optical SED for a large sample of SNe Ia might guide the theoretical investigations.

The importance of UV emission as a probe of the SN Ia event has been recognized for decades, but it has been challenging to perform rest-frame UV observations. Efforts to observe higher-z SNe Ia have increased in recent years with many large telescopes being utilized. Ellis et al. (2008) used the Low Resolution Imaging Spectrometer (LRIS) spectrograph on the Keck I telescope to observe Supernova Legacy Survey (SNLS) SNe Ia, using SNLS photometry to remove host galaxy light from the spectra (hereafter E08). E08 found that the dispersion of individual spectra about a mean mid-z spectrum increased in the UV. The mean spectrum was not found to have evolved compared to a low-z mean spectrum. Foley et al. (2008) performed an independent study that used a collection of large telescopes to observe ESSENCE mid-z SNe Ia, also finding that the spectral dispersion increased to the UV. However, uncertain galaxy contamination correction prevented a robust comparison of spectral continua. Foley et al. (2012a) employed the LRIS spectrograph on Keck to observe 21 mid-z SNe Ia from the Sloan Digital Sky Survey Supernova Survey (hereafter F12). F12 was able to remove galaxy contamination from the spectra by modeling the galaxy SED from SDSS photometry, and used a low-z sample of optical SN Ia spectra (Silverman & Filipenko 2012) combined with a sample of 46 low-z UV spectra (Foley et al. 2008). With this high-quality data set, F12 found that while the optical spectra were nearly identical, the UV portion of a mean spectrum of the mid-z Keck/SDSS sample had excess flux relative to a low-z mean spectrum.

Sullivan et al. (2009) compared a low-z mean spectrum, the E08 mid-z mean spectrum, and a high-z ($z \geqslant 0.6$ SNe with *Hubble Space Telescope* (*HST*)/ACS spectra; Riess et al. 2007) mean spectrum. There was an indication of UV flux excess for the higher redshift samples, but this was discounted because of the relatively small low-z sample used in the analysis. Cooke et al. (2011) and Maguire et al. (2012) expanded the low-z sample, paying careful consideration to selection effects; again, there were differences in the UV continuum.

A study by Balland et al. (2009) used the ESO/Very Large Telescope to observe SNLS SNe Ia, using CFHT photometry to remove host galaxy light from the spectra (hereafter B09). That work concentrated on the variation of spectral features with redshift, finding that higher-z spectra have shallower intermediate mass element absorption features. However, this was attributed to different color distributions for the samples, as the stretch values were similar given the uncertainties. Collectively, these studies show that there is little overall evolution of the optical emission with redshift, but more in the UV. The direction of that evolution is for the higher-z SNe Ia to be brighter in the UV. At a given redshift, the UV emission exhibits increased dispersion compared to the optical wavelength range. One interpretation of these findings has been improved confidence for the cosmological utility of SNe Ia in the optical wavelength range, combined with skepticism for the cosmological utility of the UV wavelength range.

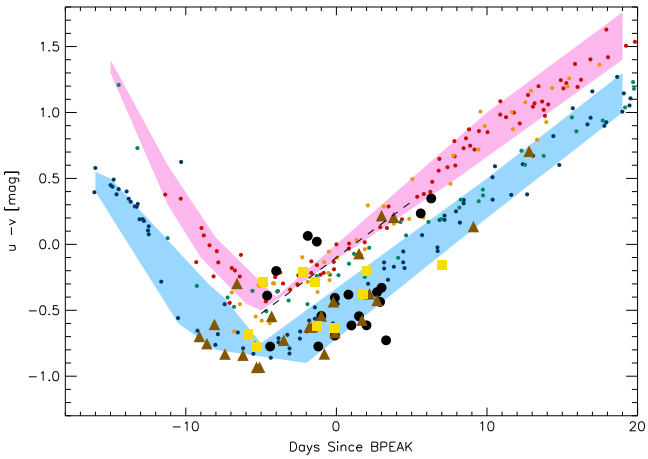

Figure 1. $u - v$ colors of low-z vs. mid-z samples. UVOT photometry is shown with small circles, and is contained in blue and red shaded regions representing the range of colors within each group. Foley et al. (2012a) mid-z spectrophotometry is shown with large black circles. Ellis et al. (2008) mid-z spectrophotometry is shown with large brown triangles. Balland et al. (2009) mid-z spectrophotometry is shown with large yellow squares. UVOT photometry is color-coded according to M13, with NUV-blue (blue), NUV-red (red), MUV-blue (orange), and irregular (green). The mid-z photometry exhibits separation into *two color curves*, as seen in the UVOT photometry in M13.

In Section 2, we compare the $u - v$ colors of low-z versus mid- and high-z photometry and spectrophotometry. In Section 3, we compare paired spectra from each group. In Section 4, we compare $u - b$ and $b - v$ colors, with Section 5 devoted to exploring the cosmological implications of the optical color differences. Section 6 summarizes these findings and argues for altering light curve fitting routines to account for the existence of two color groups.

2. COMPARING $u - v$ COLORS OF LOW-, MID- AND HIGH-Z SAMPLES

The UVOT instrument on the *Swift* satellite is executing a long-term program of observing many nearby SNe Ia in the UV and optical ranges (Brown et al. 2010, 2012; Bufano et al. 2009; Wang et al. 2009a; Milne et al. 2010, 2013; Foley et al. 2012a). In this program, the UV emission from a large sample of events (thousands of epochs of observations of more than 50 SNe Ia) is being studied to search for universal characteristics as well as for patterns in the variations that are seen. Milne et al. (2013) found that the UV-optical colors of normal SNe Ia evolve dramatically with epoch and that there exist two major color groups within the subset of normal SNe Ia. The larger, NUV-red group contained roughly two-thirds of the sample, while a second NUV-blue group was offset from the NUV-red group, evolving bluer by 0.4 mag in $u - v$ (Figure 1). The grouping was found to not correlate with peak width. Although the differences were seen in all UV filters, in this work we will concentrate on the $u - v$, $u - b$, and $b - v$ colors. The "irregular" and "MUV-blue" minor groups discussed in M13 will be treated as NUV-red in this work. The "irregular" group was concluded to be an optically broad-peaked subset of the NUV-red group, and the "MUV-blue" group had colors similar to NUV-red SNe in the $u - v$ and $uvw1 - v$ filter pairs.

Since rest-frame u and v band emission can be observed in the optical for SNe Ia at redshifts of $z \geqslant 0.2$, we utilize four studies that have obtained spectra that span the rest-wavelength range 3000–5700 Å. E08 utilized the LRIS on the Keck I telescope to obtain 36 host-galaxy subtracted spectra of 36 SNe Ia at $0.2 \leqslant z \leqslant 0.8$. Twenty-three of those spectra span 3000–5700 Å and are included in this work. The fully reduced and subtracted spectra were obtained from the Wiezmann Interactive Supernova data Repository, WISeREP (http://weizmann.ac.il/astrophysics/wiserep/). B09 utilized the FORS1 and FORS2 spectrometers to obtain 139 host-galaxy subtracted spectra of 124 SNLS SNe Ia. Ten of these spectra span 3000–5700 Å and are included in this work. The 10 spectra are in the redshift range, $0.38 \leqslant z \leqslant 0.52$. The fully reduced and subtracted "snonly" spectra were obtained from the WISeREP site. F12 utilized the LRIS spectrometer on the Keck I telescope to obtain single-epoch spectra of host-galaxy subtracted spectra of 21 SNe Ia at $0.11 \leqslant z \leqslant 0.37$. Nineteen of those spectra span 3000–5700 Å and the fully reduced and subtracted spectra are included in this work. No spectra were rejected based upon reddening selection criteria, meaning that any reddening bias would have to have been employed by the sample selection of the E08, B09, F12, and R07 publications. The UVOT-v filter has some transmission redward of 5700 Å, but we make no correction for the range of maximum wavelengths; the maximum wavelength is simply required to be 5700 Å.

The mid-z spectra were folded through the UVOT u and v transmission curves to generate spectrophotometry (Tables 1 and 2), utilizing the zero-points from Breeveld et al. (2011).[6] Figure 1 shows the spectrophotometry compared to the UVOT photometry for the low-z sample presented in M13. The mid-z data overlaps the UVOT photometry well, and exhibits a separation into two groups, as seen in the UVOT photometry. Interestingly, whereas two-thirds of the UVOT sample were NUV-red SNe Ia, there are more NUV-blue SNe Ia in the mid-z sample. A linear fit to the color evolution of the UVOT NUV-red data for epochs $|t| \leqslant 5$ days allows color evolution with time to be removed, leaving only residual magnitudes relative to the fit. Figure 2 shows a histogram of the residuals, separating the UVOT data into NUV-red/blue groups and leaving the mid-z data as a single collection. The NUV-red/blue separation is clear from the histogram, and is reproduced by the mid-z sample. The two peaks of the mid-z sample align with the two UVOT peaks, suggestive of similar colors within each group. If there is no systematic, erroneous color offset between the derivation of photometry from the low-z and mid-z samples, the alignment of peaks is suggestive of a lack of color evolution with redshift within the respective red and blue groups. The mean colors of the samples are shown in Table 3, showing that there is a consistent separation between the NUV-red and -blue groups, and that the mean colors within a group exhibit no change in color with redshift.

There are a number of factors that could cause biases in these comparisons. Imperfect host-galaxy contamination removal could produce a spectrum attributed to the SN, but brighter or fainter in some part of the spectral range. All three spectral samples utilized photometry to estimate the SN multi-band brightness against which the final spectra could be compared. Further, F12 compared the spectra of the removed emission with observed galaxy spectra, arriving at solid matches. The SNLS samples, from E08 and B09, also utilized photometry of the SN and host galaxy via the PHASE technique to extract the SN component from the reduced spectrum (see B09 for details of the method and Baumont et al. 2008). The level of agreement between the three samples suggests that host galaxy contamination does not affect the NUV-optical color group determination. As a check of the generation of UVOT spectrophotometry from spectra, we compare UVOT u and b band photometry with spectrophotometry from *HST* spectra for eight SNe Ia that were observed both with UVOT and *HST*. The *HST* spectra were presented in Maguire et al. (2011). The statistical weighted mean difference in $u - b$ was 0.04 ± 0.08 mag, due to $\Delta u = 0.02 \pm 0.12$ mag, and $\Delta b = -0.02 \pm 0.08$ mag. We conclude that there is no significant offset between the *HST* spectrophotometry and the UVOT photometry.

SNLS-04D2gc appears in both groups, based upon two different spectra, with the pre-peak spectrum suggesting NUV-red and the at-peak spectrum suggesting NUV-blue. One NUV-blue event from M13, SN 2008hv, was red enough at similar epochs to appear in the NUV-red group, so perhaps SNLS-04D2gc and SN 2008hv feature a similar anomaly in the early epoch evolution, and belong in the NUV-blue group. Alternatively, as the two spectra were obtained by different searches and were thus subjected to different host galaxy emission removal, it remains possible that the subtraction methodology introduced a bias. We note that the maximum wavelengths for both spectra fail to reach the edge of the v-filter, leaving open the possibility of missed emission. We include two SN Ia spectra that were excluded from the E08 analysis of SNLS-05D1hk & 03D4cj. Both are SN 1991T-like and appear to be similar to the other NUV-blue events at their respective epochs.[7] It is important to point out that the mid-z histograms are derived from one data point per SN, while many data points per SN can be included in the UVOT low-z histograms. The low-z UVOT and *HST* NUV-red/blue ratios are taken from M13.

Riess et al. (2007) obtained *HST* photometry and spectra of high-z SNe Ia with redshifts exceeding $z \geqslant 0.6$. None of the spectra in that study span the $u - v$ wavelength range, but the K-corrected U and V photometry can be compared to the UVOT photometry. Figure 3 shows that the high-z *HST* photometry matches the NUV-blue group with nearly all eligible SNe Ia NUV-blue (2002eb, HST05Gab, 2003xx, HST040mb, HST04Rak, 2002fw, 2003eq, HST05Dic, HST05Str). As few as zero or as many as two SNe from this sample could be NUV-red; we list SN 2002hr as NUV-red and SN 2002kd as undetermined. This suggests an even stronger dominance of NUV-blue events at high redshifts. The K-corrected photometry was used as published, with no attempt to generate separate NUV-blue and NUV-red K-corrections.

Dividing the mid-z sample into two bins based on redshift, we see that there is a transition from NUV-red dominance at low-z to NUV-blue dominance at high-z (Figure 4). The UVOT and *HST* low-z SN groupings are from M13. The mid-z groups are binned as $0.18 \leqslant z \leqslant 0.4$ and $0.4 \leqslant z \leqslant 0.53$, respectively, with 29 and 20 SNe Ia in the two mid-z bins. There are 23 UVOT SNe Ia, 23

[6] For the *ubv* filters, the Breeveld et al. (2011) zeropoints are the same as Poole et al. (2008).

[7] SNLS-03D3bb was excluded from this sample, as it is a super-Chandrasekhar candidate. It also appears to be similar to NUV-blue SNe Ia, as was the super-Chandrasekhar candidate, SN 2009dc, featured in M13. Brown et al. (2014) concentrates on UVOT-observed super-Chandrasekhar candidates.

Table 1
Colors of Mid-z SN Ia Samples

SN Name	Sample[a]	Epoch (days)[b]	z (km s^{-1})	s/Δ[c]	$E(B\text{-}V)$/c[d] (mag)	λ(min) (mag)	λ(max) (Ang.)[e]	v(Si II)$_0$ (Ang.)[e]	$u-v$ (mag)[f]	$u-b$ (mag)[f]	$b-v$ (mag)[f]
				NUV-blue							
03D1au	E08	−1.6	0.504	1.13(02)	0.02(03)	2476.2	5936.3	⋯	−0.63	−0.56	−0.07
03D1dj	E08	−1.8	0.400	⋯	⋯	2675.0	6389.3	⋯	−0.63	−0.46	−0.16
03D3aw	E08	−0.8	0.449	1.066(33)	−0.06(04)	2584.5	6162.9	⋯	−0.83	−0.48	−0.35
03D3ay	E08	−1.0	0.371	1.054(30)	−0.018(36)	2728.1	6521.3	⋯	−0.54	−0.48	−0.06
03D3bh	E08	−3.5	0.249	⋯	⋯	2991.4	7152.0	−11.5697	−0.73	−0.65	−0.08
03D3cc	E08	9.1	0.463	⋯	⋯	2567.2	6122.2	⋯	0.13	−0.18	0.31
03D3cd	E08	−6.2	0.461	1.19(09)	−0.00(05)	2567.3	6130.6	⋯	−0.84	−0.74	−0.10
03D4ag	E08	−5.3	0.285	1.09(02)	−0.03(02)	2911.2	6974.4	−9.44703	−0.93	−0.82	−0.12
03D4cj	E08	−7.4	0.270	1.12(01)	−0.05(02)	2944.9	7047.2	⋯	−0.83	−0.69	−0.14
04D1hd	E08	1.7	0.369	1.07(01)	−0.06(02)	2736.0	6527.6	−11.1098	−0.57	−0.55	−0.02
04D1pg	B09	−1.3	0.515	1.10(02)	0.12(04)	2811.0	5860.5	⋯	−0.62	−0.47	−0.14
04D1rh	E08	2.7	0.435	1.11(03)	−0.02(03)	2599.5	6226.9	⋯	−0.43	−0.47	0.04
04D2fp	B09	1.8	0.415	1.03(02)	−0.00(03)	3010.5	6296.7	⋯	−0.38	−0.30	−0.08
04D2gc	E08	−0.2	0.522	1.12(03)	0.05(04)	2457.9	5875.4	⋯	−0.44	−0.51	0.07
04D4in	E08	−5.1	0.516	1.17(02)	−0.04(03)	2463.7	5890.5	⋯	−0.93	−0.82	−0.11
04D4jr	B09	−5.9	0.470	1.15(02)	−0.02(03)	2896.9	6039.7	⋯	−0.68	−0.60	−0.08
04D4jr	E08	−0.1	0.482	1.15(02)	−0.02(03)	2520.2	6029.0	⋯	−0.67	−0.57	−0.10
2005ik	F12	3.0	0.320	0.872(68)	0.03(10)	2521.9	7001.9	⋯	−0.33	−0.45	0.12
2005ix	F12	2.9	0.260	0.971(39)	0.01(01)	2740.5	7335.3	−13.1845	−0.44	−0.39	−0.05
2005jc	F12	0.8	0.215	0.995(27)	0.12(04)	2739.9	7607.0	−10.6360	−0.38	−0.33	−0.06
2005jd	F12	2.7	0.320	1.090(52)	0.01(01)	2659.9	7001.9	−10.8679	−0.36	−0.37	0.01
2005ji	F12	1.0	0.214	−0.07(09)	0.01(02)	2775.1	7613.3	−9.82174	−0.62	−0.49	−0.12
2005jl	F12	−0.1	0.180	1.003(32)	0.10(03)	2783.9	7832.7	−10.2749	−0.69	−0.68	−0.01
2005jn	F12	3.3	0.330	1.025(56)	0.01(01)	2557.1	6949.3	−8.84449	−0.73	−0.74	0.01
2005jo	F12	−1.0	0.230	1.055(39)	0.14(07)	2932.5	7514.3	−9.54432	−0.54	−0.35	−0.20
05D1ix	E08	−9.1	0.490	1.06(02)	−0.04(03)	2503.4	6003.4	⋯	−0.70	−0.48	−0.22
05D1hk	E08	−8.6	0.263	1.15(02)	0.01(03)	2957.0	7065.9	⋯	−0.75	−0.78	0.03
05D1iy	E08	−8.1	0.248	⋯	⋯	2997.3	7164.6	⋯	−0.61	−0.75	0.14
05D2ac	B09	2.0	0.479	1.11(02)	−0.01(03)	2879.5	6003.2	⋯	−0.20	−0.31	0.11
05D2bv	B09	−0.1	0.474	0.99(01)	−0.09(03)	2889.6	6023.9	⋯	−0.63	−0.46	−0.18
05D2dw	B09	−5.3	0.417	1.11(02)	0.02(03)	3005.3	5736.4	⋯	−0.78	−0.53	−0.25
05D4cw	B09	7.0	0.375	0.91(01)	−0.10(03)	3097.4	6457.4	⋯	−0.15	−0.15	−0.00
2006pf	F12	2.0	0.366	−0.32(10)	0.01(01)	2358.6	6775.4	⋯	−0.61	−0.82	0.21
2006pq	F12	−4.4	0.193	−0.36(13)	0.04(04)	2651.2	7755.7	−10.8753	−0.77	−0.66	−0.11
2007lu	F12	−0.1	0.319	−0.47(07)	0.17(04)	2434.4	6975.4	−11.7068	−0.41	−0.51	0.10
2007lw	F12	1.5	0.290	−0.23(09)	0.01(02)	2569.7	7130.6	−10.8118	−0.54	−0.46	−0.09
2007qu	F12	−1.2	0.310	−0.25(14)	0.01(01)	2466.4	7009.6	−10.4310	−0.77	−0.79	0.02
				NUV-red							
03D3af	E08	3.0	0.532	⋯	⋯	2444.5	5829.0	⋯	0.22	−0.09	0.31
03D3bl	E08	3.8	0.355	1.02(02)	0.24(03)	2759.5	6596.3	−11.2125	0.20	0.00	0.20
04D2gc	B09	−4.9	0.521	1.12(03)	0.05(04)	2800.1	5857.3	⋯	−0.29	−0.36	0.08
04D3ez	E08	1.5	0.263	0.89(01)	0.07(03)	2961.2	7074.4	−10.6360	−0.07	−0.22	0.15
04D3fk	E08	−6.6	0.357	0.95(01)	0.10(02)	2754.5	6587.9	−12.7075	−0.30	−0.34	0.05
04D4ju	B09	−2.2	0.472	1.05(02)	0.18(03)	2893.2	6031.7	⋯	−0.21	−0.25	0.04
2005jm	F12	−4.6	0.204	1.079(39)	0.17(09)	2809.8	7676.5	−12.0008	−0.39	−0.35	−0.04
2005jp	F12	−1.3	0.213	1.017(43)	0.23(04)	2779.5	7620.8	−13.7803	0.02	−0.15	0.17
05D2mp	E08	−4.3	0.354	1.14(03)	0.05(04)	2762.8	6596.7	−12.2951	−0.55	−0.55	0.00
2006pt	F12	−1.9	0.299	−0.34(17)	0.08(11)	2436.4	7122.8	−11.5844	−0.06	−0.22	0.28
06D4cq	B09	−1.4	0.411	1.04(01)	−0.01(02)	3017.5	5760.3	⋯	−0.29	−0.20	−0.09
2007ml	F12	−4.0	0.190	−0.08(09)	0.17(04)	2706.7	7729.9	−12.4129	−0.20	−0.21	0.01
				Undetermined							
2006pz	F12	5.6	0.325	−0.25(14)	0.08(08)	2560.7	6983.0	⋯	0.23	0.04	0.19
2005jk	F12	6.3	0.190	0.927(35)	0.22(03)	2846.2	7766.8	−11.7950	0.35	0.16	0.18
03D3ba	E08	12.8	0.291	1.09(02)	0.14(04)	2896.5	6916.0	⋯	0.71	0.22	0.49

Notes.
[a] E08—Ellis et al. (2008), B09—Balland et al. (2009), F12—Foley et al. (2012a).
[b] Epoch of spectrum relative to B-band maximum.
[c] Δ or stretch (s) parameter for SN light curves. Stretch is from Guy et al. (2010), Δ (bold font) is from F12.
[d] $E(B-V)$ or color (c) parameter for SN light curves. Color (c:bold font) is from Guy et al. (2010).
[e] Minimum and maximum rest-frame wavelengths of spectrum.
[f] Color of spectrophotometry.

Table 2
Mean Color Residuals of Samples

	$\Delta(u-v)$[a] (mag)		$\Delta(u-b)$[a] (mag)		$\Delta(b-v)$[a] (mag)	
	low-z	mid-z	low-z	mid-z	low-z	mid-z
NUV-red	0.04 ± 0.09	0.09 ± 0.14	0.19 ± 0.07	0.17 ± 0.09	-0.00 ± 0.04	0.05 ± 0.10
NUV-blue	-0.38 ± 0.06	-0.48 ± 0.15	-0.15 ± 0.07	-0.21 ± 0.15	-0.10 ± 0.08	-0.12 ± 0.11

Note.
[a] Residual colors relative to fits described in the text.

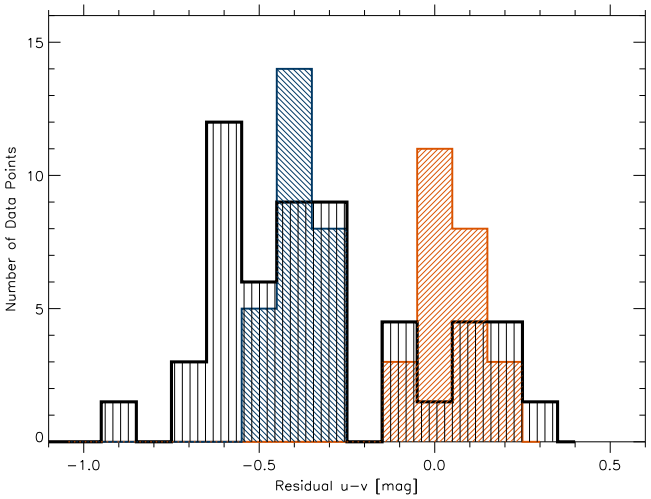

Figure 2. Histogram of residuals of low- and mid-z $u-v$ photometry vs. a linear fit to the UVOT NUV-red photometry. UVOT NUV-red photometry is shown in red with diagonal lines. UVOT NUV-blue photometry is shown in blue with blue diagonal lines. Mid-z spectrophotometry is shown with thick black vertical lines, scaled up by 1.5. The low- and mid-z histograms peak at similar colors, with a switch from more NUV-red photometry at low-z to more NUV-blue spectrophotometry at mid-z. Linear fit was for $|t - t_{\rm BPEAK}| \leqslant 6$ days.

Table 3
Change with Redshift of NUV-red vs. NUV-blue Ratio

SN Sample	N(Red)[a]	N(Blue)[a]	Perc. Blue	Δ(Perc. Blue)[b]
UVOT	16	7	30	11
low-z HST	15	8	35	10
mid-$z \leqslant 0.4$	8	21	72	14
mid-$z \geqslant 0.4$	4	16	80	20
high-z	1	9	90	27

Notes.
[a] Number of SNe Ia in sample determined to be NUV-red or NUV-blue.
[b] Poisson error of percentages, additionally accounting for SNe with uncertain determinations.

HST low-z SNe Ia, and 10 *HST* high-z SNe Ia, as shown in Table 4. A more quantitative discussion of UV dispersion is presented at the end of Section 3.

The shift from dominance of NUV-red events at low-z to dominance of NUV-blue events at mid-z is suggestive of a fundamental change in the properties of SNe Ia with redshift. Both the Maguire et al. (2012) and the F12 low-/mid-z spectral studies reported that the UV-optical colors were bluer for the mid-z sample. The photometry comparisons suggest that the reason for the bluer colors at mid-z is the dominance of NUV-blue SNe Ia instead of NUV-red SNe Ia at mid-z. It is also quite reasonable to understand that generating a mean spectrum from a combination of NUV-red and -blue SNe Ia will lead to a UV wavelength range featuring much more scatter. Two samples which have mean colors that differ by 0.4 mag are being treated as a single group in those studies.

One alternative explanation to NUV-blue SNe Ia being the dominant explosion variety at higher redshifts is that the NUV-blue events are more luminous and are over-represented in a magnitude-limited sample. There are a number of factors that argue against that explanation. First, none of the samples were rest-frame u-band-dominated when determining candidates, so a luminosity bias would only occur if NUV-blue SNe were optically bright. The fact that this separation was not recognized years ago argues against a difference of more than 0.1–0.2 mag. Further, E08 and F12 studied magnitude selection effects and determined that their samples were not strongly biased. Second, all three mid-z surveys showed the same NUV-blue dominance, despite the differences between the sample selection for each survey. Third, even if there were a luminosity bias of 0.3 mag, the effect would be much too small to shift the NUV-blue:red ratio from 40% to 90%. We conclude that there is a real variation in the NUV-blue to NUV-red ratio with redshift.

3. SPECTRAL COMPARISONS OF NUV-RED AND NUV-BLUE SNE IA

Using the same approach as employed for the low-z *HST* SN spectra in M13, we compare spectra of NUV-red/blue pairs. For two SNe to be considered "pairs," we require that they have similar optical light-curve shapes (in the same third of the sample), have similar phases (within 1 day excepting one pair), and have *different* UV colors. Selecting the best matches that meet these requirements allows a direct comparison of SN spectra which largely removes possible differences attributable to light-curve shape (and thus luminosity) and phase; therefore, any differences in the spectra are more likely to be related to the differences in UV colors. We present these spectra pairs in Figure 5.

As expected, the spectra of SNe from the NUV-blue group have a higher UV flux than those of SNe from the NUV-red group. Interestingly, there is no noticeable difference in the optical continua ($\lambda \gtrsim 4500$ Å) of SNe from the two groups. This is perhaps not unexpected given the similar optical colors for all SNe. But it indicates that this effect is not caused by odd reddening, which would have some subtle difference in the optical continuum, or the confluence of a strong continuum difference offset by differences in spectral features.

Also notable is that the same UV spectral features are present for both groups. Although the strengths of these lines are different for each SN, it is clear that the UV color difference is

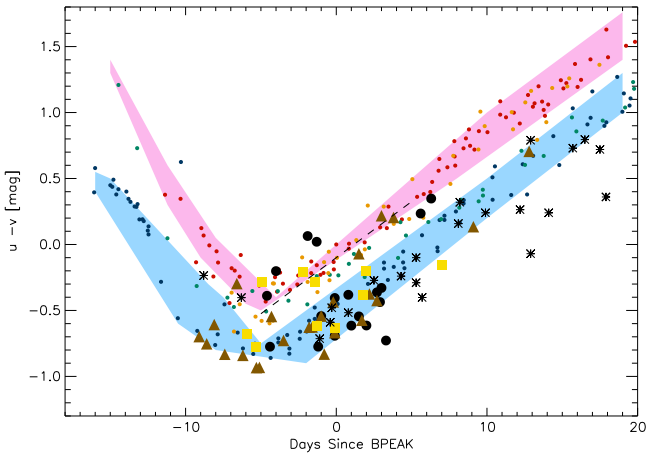

Figure 3. $u - v$ colors of low-z, mid-z, and high-z samples. UVOT photometry is shown with small circles. Foley et al. (2012a) high-z spectrophotometry is shown with large, black circles. Ellis et al. (2008) high-z spectrophotometry is shown with large, brown triangles. Balland et al. (2009) mid-z spectrophotometry is shown with large, yellow squares. Riess et al. (2007) *HST* photometry is shown with black stars. UVOT photometry is color-coded according to M13, with NUV-blue (blue), NUV-red (red), MUV-blue (orange) and irregular (green). The high-z photometry exhibits similar color curves, as seen in the low- and mid-z photometry.

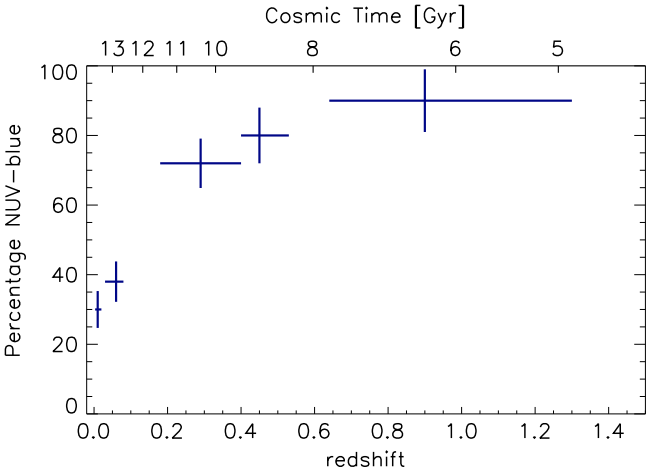

Figure 4. Percentage of NUV-blue SNe Ia vs. all SNe Ia as a function of redshift. At low-z, there are more NUV-red events, but with increasing redshift, the NUV-blue events become the dominant group.

the result of a difference in a wide band in the UV wavelength range and not the presence/absence of particular lines or dramatically different line strengths (and unaffected UV continua) in one particular group.

The final clear difference between the two groups is the velocity of multiple spectral features. When the Si II λ6355 feature is observed with a reasonable signal-to-noise ratio (S/N), the NUV-red SN often has a broader, higher-velocity line than the NUV-blue paired SN (and the NUV-blue spectrum never has a higher-velocity feature for our pairs). This is sometimes easier to see in the residual spectra, which shows a positive bump at ~6100 Å, indicating excess absorption in the NUV-red spectra. This is perhaps best seen in the comparison of SNe 2006pq and 2007ml. Since the SNe have similar light-curve shapes and the spectra are at similar phases, we conclude that the velocity of the Si II λ6355 feature is linked to the UV colors. We note that the trend with velocity is not exclusive to Si II; in particular, Ca II H&K shows similar behavior.

Foley & Kasen (2011) first showed that the intrinsic $B_{\rm max} - V_{\rm max}$ color of a SN Ia was strongly linked to the velocity of the Si II λ6355 feature near maximum light. The physical explanation for this effect is that higher-velocity spectral features are also broader, creating additional opacity in the blue where line blanketing dominates. Farther to the red, electron scattering dominates the opacity, and thus the broader lines do not increase the overall opacity for those wavelengths. This interpretation predicts that other than the obvious velocity differences, spectral differences between low- and high-velocity SNe should be largely constrained to the bluer wavelengths, that the differences should largely be a difference in the continuum, and that the differences should persist to the UV. Figure 5 supports this interpretation, and the differences in UV colors may predominantly be caused by different opacities resulting from different ejecta velocities. With a larger UVOT sample, an interesting comparison will be between Low Velocity (LV) NUV-blue SNe and LV NUV-red SNe. If the Si II velocity distributions are similar between those groups, the prediction would be that the $b - v$ colors would be similar.

Thomas et al. (2011) reported a correlation between UVOT NUV-blue SNe Ia and the detection of an absorption feature at λ6580 attributed to C II. M13 confirmed the correlation for all seven UVOT NUV-blue SNe in the sample. Since the λ6580 feature is only detected at early epochs ($t \lesssim -4$ days) in normal SNe Ia, one would only expect to detect this feature in early epoch spectra that reach to 6650 Å. Six mid-z spectra meet those criteria. The comparison spectra of the NUV-blue SN 2006pq shows a notch at the location of the C II feature, when compared with the NUV-red SN 2007ml, but in general the spectra either cut off before the C II feature, were of too low S/N, or were obtained at too late an epoch for C II identification. There are therefore too few SNe from which we can draw strong conclusions. However, several groups have found that high-velocity SNe Ia, which we associate with NUV-red objects, are far less likely to have detectable C II (Folatelli et al. 2012; Parrent et al. 2011; Silverman & Filippenko 2012), consistent with the findings of M13.

F12 generated mean spectra of low-z and mid-z samples and determined that when normalized to the optical emission, the mid-z mean spectrum featured a UV excess, the same result that was found by Maguire et al. (2012). Recognizing the increased fraction of NUV-blue events at mid-z and the similarities of the distributions of low-z and mid-z colors within the red/blue groups (shown in Figure 2), the comparison of mean spectra can be revisited with the additional separation between NUV-red and -blue SNe. We note that several of the spectra used here were also used by F12.

We used the methods of Foley et al. (2008) and F12 to generate mean spectra and uncertainty spectra corresponding to the boot-strap resampling uncertainty. Using only spectra near peak brightness ($|t_{\rm BPEAK}| \leqslant 7$ days) and normalizing in the rest-frame wavelength region 4500 Å $\leqslant \lambda \leqslant$ 7500 Å, mean spectra for the low-z sample (Foley et al. 2012c) and mid-z NUV-red and NUV-blue samples are presented in Figures 6–8.

Comparing the mean mid-z NUV-red and low-z mean spectra (Figure 6), we see that the spectra are nearly identical. There are two clear differences: the mid-z NUV-red has broader and higher-velocity Si II λ6355 and Ca H&K features. The difference in the Ca H&K feature is exclusively to the blue portion of the complex feature (Foley & Kirshner 2013), which has a significant contribution from

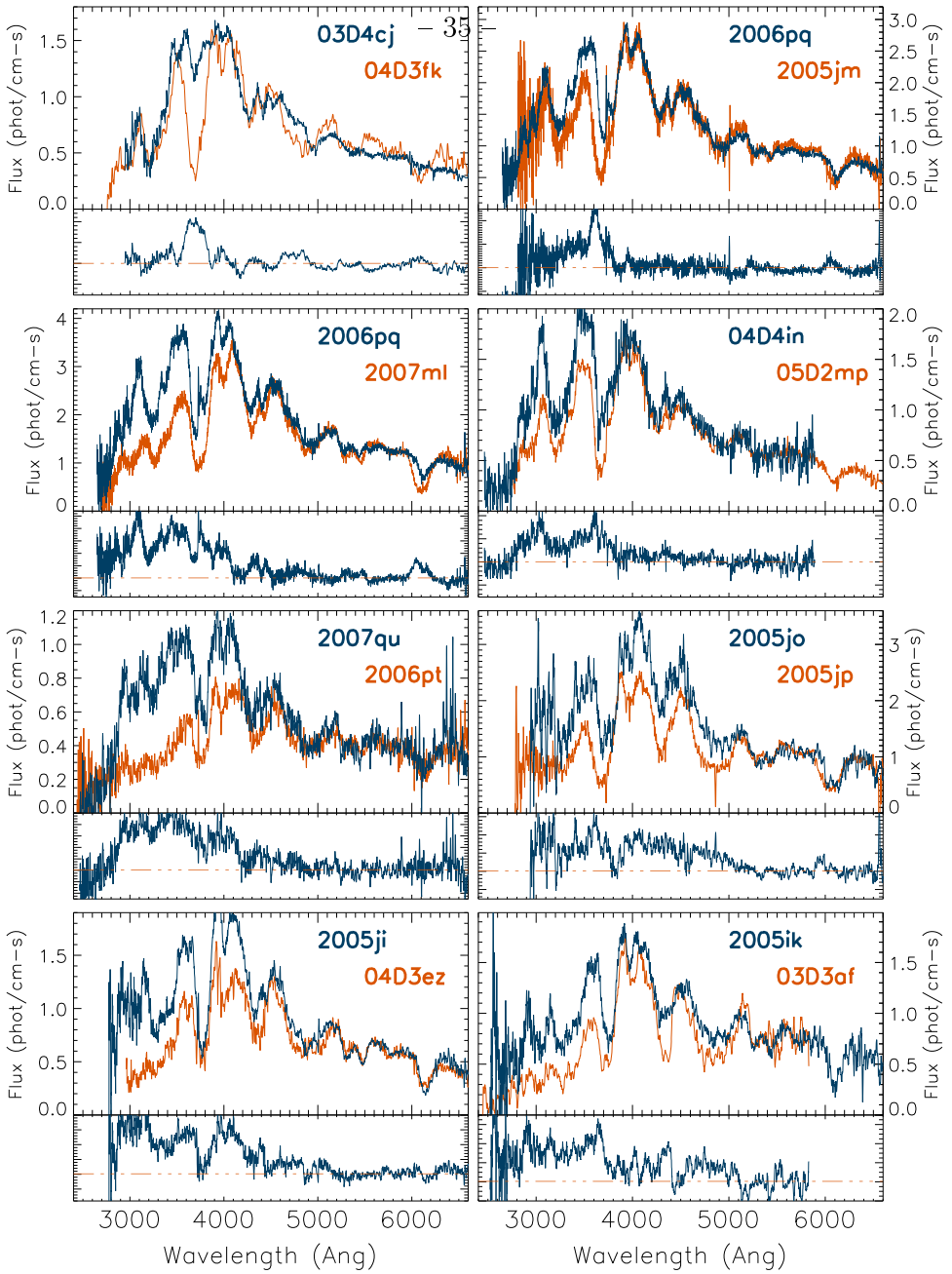

Figure 5. Comparisons of NUV-blue and -red SN spectra from Ellis et al. (2008), Balland et al. (2009) and Foley et al. (2012a) mid-z samples. Solid blue lines are NUV-blue events, red-dashed lines are NUV-red events. The spectra are normalized to the overlap in the 5000–6000 Å wavelength range, or to the red edge of the spectrum. Below each spectrum is the residual spectrum of the NUV-blue minus NUV-red. Spectra were matched in epoch and peak width. Normalizations that do not reach 6000 Å are apparent in the residual spectra.

Si II λ3727 (but also see Childress et al. 2013). As the low-z sample has both NUV-red and NUV-blue SNe, one can extrapolate from the previous comparison of pairs that the relatively small difference in velocity is the result of the NUV-blue SNe in the low-z sample.

Another difference in the mid-z NUV-red and low-z mean spectra is the strength of the 4800 Å feature, with the mid-z NUV-red mean spectrum having a weaker absorption than that of the low-z mean spectrum. Foley et al. (2008) reported a similar difference in a comparison of low-z and mid-z mean spectra. This feature is predominantly caused by Fe II absorption with additional absorption from Si II and Fe III. Because of the blending of this feature, there are multiple plausible explanations for such a difference ranging from excitation/temperature differences to differences in composition.

Examining Figure 7, we see more dramatic differences between the mid-z NUV-blue and low-z mean spectra. The mean mid-z NUV-blue spectrum has lower velocity features, a UV excess, and weaker spectral features compared to the mean low-z spectrum. Specifically, the mid-z NUV-blue mean spectrum has excess flux compared to the low-z mean spectrum for wavelengths shorter than ~4000 Å. This is consistent with what has been seen in other comparisons (Cooke et al. 2011; Maguire et al. 2012, F12) and supports the suggestion that the spectral evolution with redshift is dominated by the change in

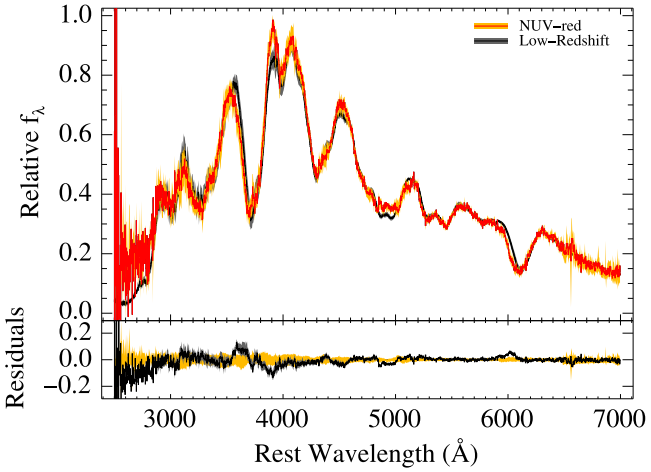

Figure 6. Mean spectra from high-z NUV-red SNe Ia compared with the mean low-z spectrum. The red spectrum is the mid-z NUV-red mean spectrum, the black spectrum is the mean low-z spectrum (F12). The spectral samples are limited to near-peak epochs, $|t_{\rm BPEAK}| \leqslant 7$ days, and are normalized over the 4500 Å $\leqslant \lambda \leqslant$ 7500 Å wavelength region. The two spectra approximately agree.

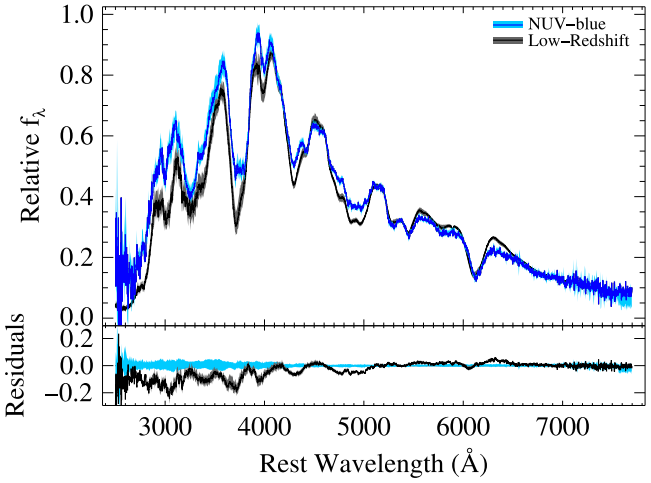

Figure 7. Mean spectra from mid-z NUV-blue SNe Ia compared with the mean low-z spectrum. The blue spectrum is the mid-z NUV-blue mean spectrum, and black spectrum is the mean low-z spectrum (F12). The spectral samples are limited to near-peak epochs, $|t_{\rm BPEAK}| \leqslant 7$ days, and are normalized over the 4500 Å $\leqslant \lambda \leqslant$ 7500 Å wavelength region. The NUV-blue spectrum exhibits a UV excess relative to the mean low-z spectrum.

membership from NUV-red events at low-z to NUV-blue events at high-z.

Most spectral features in both the UV and optical, including the Ca H&K feature, the "Mg II 4300" feature, and the 4800 Å feature, are weaker in the mid-z NUV-blue mean spectrum. In retrospect, a similar behavior can be seen between the intermediate-redshift and low-redshift mean spectra of F12. Considering that many of the same spectra contribute to the F12 mean spectra and the mean spectra presented here, this observation is reassuring. Intriguingly, the lower ($\overline{z} = 0.19$) and higher ($\overline{z} = 0.31$) redshift subsamples presented by F12 also show this trend, with the higher redshift mean spectrum having muted features relative to the lower redshift mean spectrum.

We compare the mean mid-z NUV-blue and NUV-red spectra in Figure 8; as expected, there are significant spectral differences: the NUV-blue spectrum has lower velocity

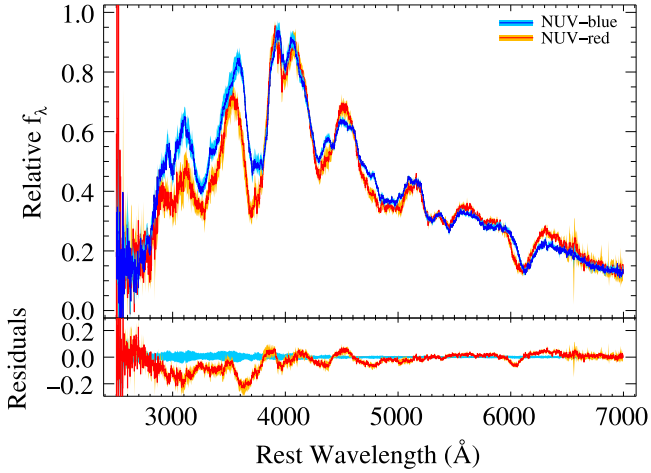

Figure 8. Mean spectra from high-z SNe Ia separated into NUV-red and NUV-blue groups. The red spectrum is the high-z NUV-red mean spectrum, the blue spectrum is the mid-z NUV-blue mean spectrum. The spectral samples are limited to near-peak epochs, $|t_{\rm BPEAK}| \leqslant 7$ days, and are normalized over the 4500 Å $\leqslant \lambda \leqslant$ 7500 Å wavelength region. The NUV-blue mean spectrum is bluer in the UV wavelength.

features, a UV excess, and weaker spectral features. Since the mid-z NUV-red mean spectrum was similar to the low-z mean spectrum, most of the above discussion between the mid-z NUV-blue mean spectrum and the low-z mean spectrum also applies to this comparison.

The wavelength of maximum absorption for the Si II λ6355 feature corresponds to a blueshifted velocity, $v_{\rm Si\,II}$, of $-10{,}960 \pm 160$ km s^{-1} and $-12{,}280 \pm 80$ km s^{-1}, for the NUV-blue and NUV-red mean spectra, respectively. For a subset of the individual mid-z spectra, we were able to measure $v_{\rm Si\,II}$, and its value at B-band maximum brightness, $v^0_{\rm Si\,II}$ (Foley et al. 2011). The NUV-blue and NUV-red samples had average $v^0_{\rm Si\,II}$ of $-10{,}630$ and $-11{,}850$ km s^{-1}, respectively. Similarly, the two groups had median values of $-10{,}620$ and $-11{,}740$ km s^{-1}, respectively. The velocity difference in the mean spectra is duplicated in measurements of individual objects. All measurements suggest that the NUV-red sample has an average ejecta velocity that is ∼12% larger than that of the NUV-blue sample.[8]

Of the 15 NUV-blue SNe for which we could determine $v^0_{\rm Si\,II}$, 14 have velocities below $-11{,}800$ km s^{-1}, the nominal separation between "high-velocity" and "LV" SNe Ia (Foley & Kasen 2011). In contrast, four of the eight NUV-red SNe for which we could measure $v^0_{\rm Si\,II}$ had a velocity higher than $-11{,}800$ km s^{-1}. M13 found similar results for the low-z sample: the NUV-blue objects exclusively had LV ejecta, while half of the NUV-red objects were found in each group. Performing a Kolmogorov–Smirnov test, we find that the NUV-blue and NUV-red SNe likely have different parent populations with respect to ejecta velocity ($p = 0.0027$). By contrast, performing a Kolmogorov–Smirnov test on the stretch values, we find that the NUV-blue and NUV-red SNe likely have similar distributions of stretch values ($p = 0.87$).

We also examined the pseudo-equivalent width (pEW) of the Si II λ4131 feature, which has been proposed as an indicator

[8] The Si II λ6355 line velocities are all blueshifted, and thus negative, but "above" and "below" will be relative to the absolute magnitude of the velocities.

of Si II velocity and color, and is a possible way to further reduce Hubble scatter (e.g., Arsenijevic et al. 2008; Blondin et al. 2011; Nordin et al. 2011). Specifically, SNe with higher Si II λ4130 pEW tend to have higher maximum-light velocities and redder colors, as one would expect given the velocity-color relation (Foley & Kasen 2011). For the low-z, NUV-blue, and NUV-red composite spectra, we measure pEWs of 8.0, 6.4, and 11.4 Å, respectively, with an estimated systematic uncertainty of ~2.0 Å that greatly dominates over any statistical uncertainty. This measurement is consistent with NUV-blue SNe being intrinsically bluer and having lower eject velocities than NUV-red SNe.

Reconcentrating on the general features of the mean spectra, the mid-z NUV-blue and NUV-red mean spectra clearly differ in the NUV when normalized in the optical wavelength range. The differences invite the question of whether the higher dispersion reported in mean UV spectra is wholly due to a failure to separate the SNe Ia into red and blue groups. Comparing the dispersion in an optical band (4500–5500 Å) with a NUV band (3000–3500 Å) for the low-z mean spectrum, we find the NUV dispersion to be 4.2 times the optical dispersion. By constrast, that ratio is 2.8 for the mid-z NUV-blue mean spectrum and 2.7 for the mid-z NUV-red mean spectrum. Stated a different way, the NUV-blue and NUV-red mean spectra retain 68% and 63% of the NUV dispersion after separation compared to the low-z (unseparated) mean spectrum. This suggests that there remains intrinsic dispersion within each group that is independent of NUV-red/blue group membership, but that recognizing the group membership makes the NUV wavelength range closer to being useful relative to the optical wavelength range.

4. COMPARING $u - b$ AND $b - v$ COLORS OF LOW- AND HIGH-Z SAMPLES

Utilizing the $u - v$ colors to determine NUV-red versus NUV-blue membership allows the differences in the $u - b$ and $b - v$ colors to be studied. Figure 9 shows the $u - b$ color curves of the mid-z sample compared to UVOT photometry. The figure is similar to Figure 1, but the mid-z spectrophotometry has been color-coded red or blue based upon the NUV-red/blue determinations shown in Table 1. A linear fit to the NUV-red UVOT photometry is shown as a dashed line, as was performed in M13. The line was fitted for epochs $|t| \leqslant 6$ and offset to the blue by 0.2 mag so that there is a sign change between NUV-red/blue groups.[9] Histograms of the residuals to that fit are shown in Figure 10. There is still a color difference between the two groups, but it is less than for the $u - v$ colors. Table 2 shows the lower separation between NUV-red/blue, which lowers *from 0.42 and 0.57 mag to 0.34 and 0.38 mag, respectively, for the low-z and mid-z samples*, but again shows no evolution of color with redshift within a group.

The same method can be employed to study $b - v$ colors. Figures 11 and 12 show the color curves and resulting histograms for the $b - v$ colors. A quadratic fit is utilized for the $b - v$ photometry, using data during the $|t| \leqslant 10$ day epoch. The NUV-red and NUV-blue distributions are less separated, with overlap for both samples. Table 2 again shows the lower separation between NUV-red/blue, which lowers to 0.10 and 0.17 mag for the low-z and mid-z samples, but yet again shows no evolution of color with redshift within a group.

[9] The linear fit was not started at earlier epochs to avoid the abrupt early color change. The linear fit was not extended to later epochs to avoid NUV-blue/irregular confusion, as discussed in M13.

5. COSMOLOGICAL IMPLICATIONS OF NUV-RED/BLUE $b - v$ COLOR DIFFERENCES

The difference in $b - v$ colors for NUV-red versus NUV-blue SNe Ia, combined with the change of their relative fraction with redshift, could potentially bias cosmological measurements. This is because accurate SN distances require correcting for dust extinction, which is inferred from the colors of SNe, particularly the $B - V$ color at high z. While we cannot measure the precise strength of this effect from the relatively small sample of SNe IA with UVOT imaging, here we make a first attempt to understand the potential bias associated with a SN population whose intrinsic color properties change, on average, with redshift.

SN Ia distance-fitting algorithms measure the observed color for a SN, compare that color to a fiducial model that was trained mostly on low-z data, and, using an empirical relation (guided by dust reddening in some algorithms), determine a luminosity correction. SNe with redder inferred colors are given a larger correction. Since the fiducial model is trained primarily on low-z SNe, this paper argues that it is likely to be optimized for the NUV-red SNe Ia that dominate in the local universe. When such a model is applied to high-z SNe Ia, which have a much larger fraction of NUV-blue SNe, the inferred colors will be, on average, biased blue. As a result, high-z SNe Ia may, on average, have measured luminosities which are biased low. Ideally, a distance-fitting algorithm would be developed to separately treat NUV-red and NUV-blue SNe Ia. At the current time that is not possible, because the discrimination we present is based on information that is not available for the majority of the SNe Ia in either the nearby, training data set(s) or the distant, cosmological data set(s). The situation is made still more complicated, because there are many covariances and competing effects when making a distance measurement (Foley et al. 2012c), and the magnitude and covariance of different effects all change with redshift. In this section, we perform a simple, but realistic, simulation of this effect and determine, roughly, the ultimate effect of the changing demographics of SNe Ia on measuring cosmological parameters.

Without determining the absolute magnitudes that separate NUV-blue from NUV-red SNe Ia, we do not know the exact bias that results from treating both groups as a single sample. However, making the assumption that the absolute optical magnitudes are the same, we can assess the impact of this potential bias. To do this, we perform two similar simulations. For both, we assume that the two groups have a difference in $b - v$, $\Delta(b - v)$, that directly impacts the distance modulus such that $\Delta\mu = \Delta A_V = R_V \Delta(b - v)$ (note that the sign of this value is set this way because we defined $\Delta(b - v) > 0$). The average Hubble residual bias is then

$$\mathrm{HR} = 0.5 * \Delta\mu / \left(f_b - f_r\right) \quad (1)$$

$$= 0.5 * \Delta\mu / \left(2f_b - 1\right), \quad (2)$$

where f_b and f_r are the fraction of NUV-blue and NUV-red SNe, and assuming that $f_b + f_r = 1$. We then use the fractions of NUV-blue and NUV-red SNe as determined in Section 2 to determine the evolution of the Hubble residual bias as a function of redshift.

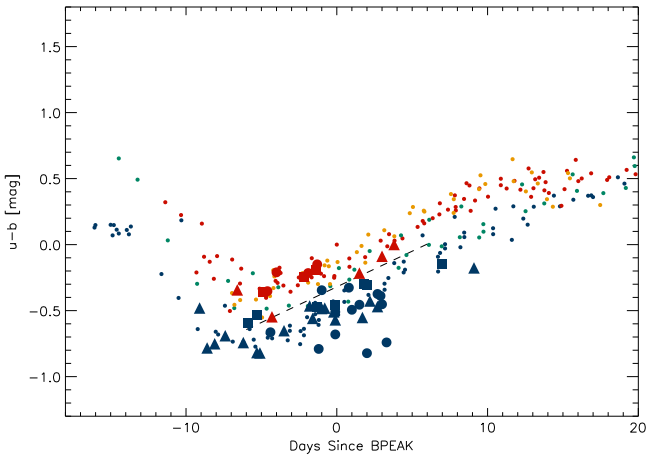

Figure 9. $u - b$ colors of low-z vs. mid-z samples. Figure symbols are similar to Figure 3 except the mid-z SNe Ia are color coded red or blue to match NUV-red/blue determinations from $u - v$ spectrophotometry.

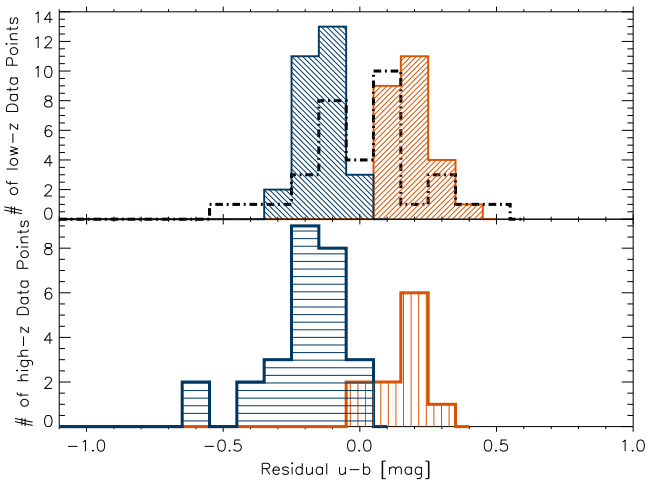

Figure 10. Histogram of residuals of low- & mid-z $u - b$ photometry vs. a linear fit to the UVOT NUV-red photometry offset to the blue by 0.2 mag. The upper panel shows UVOT NUV-red photometry (red), UVOT NUV-blue photometry (blue), and *HST* spectrophotometry from M13 (black dashed). The lower panel shows mid-z spectrophotometry with NUV-red SNe Ia (red/vertical) and NUV-blue SNe Ia (blue/horizontal). The NUV-red/blue groups are separated at both redshifts, but with less separation than the $u - v$ photometry. The low- and mid-z histograms peak at similar colors. Linear fit was for $|t - t_{\rm BPEAK}| \leqslant 6$ days.

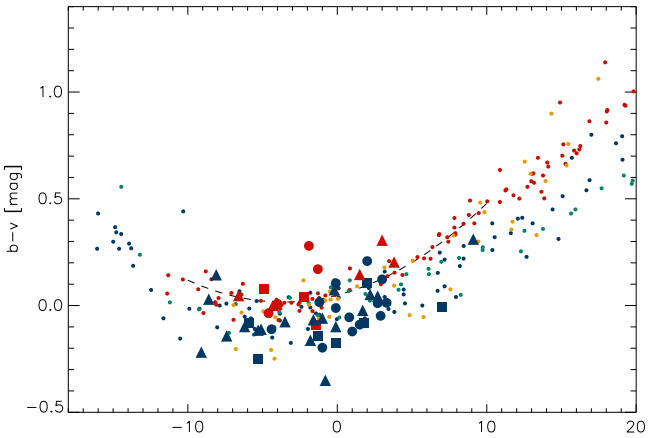

Figure 11. $b - v$ colors of low-z vs. mid-z samples. Figure symbols are similar to Figure 3.

The first simulation assumes $\Delta(b - v) = 0.10 \pm 0.09$ or $\Delta(b - v) = 0.17 \pm 0.15$, the differences seen for the low-z and mid-z samples, respectively. We also assume that $R_V = 2$ or 3.1, resulting in four distinct possibilities for the Hubble residual bias. Since there is no specific preference for one possibility over the others, we perform a Monte Carlo simulation that draws from each of the four possibilities to determine the median bias and the uncertainty on the bias.

The second simulation is similar to the first, but uses $\Delta(b - v) = 0.059 \pm 0.013$. This is the measured $B_{\rm max} - V_{\rm max}$ offset between the low and high-velocity subsamples of the Foley & Kasen (2011) sample. As shown above, ejecta velocity is highly correlated with NUV color. Although this color difference may not be exactly the difference between the NUV color subclasses, it is illustrative because of the proportionally small uncertainty for the color difference. For this simulation, we also use both values of R_V and perform a Monte Carlo simulation to determine the final bias and uncertainty.

Figure 13 shows the results of the simulations. The Hubble residuals shown are relative to a sample that has equal numbers of NUV-blue and NUV-red SNe. Both predict the Hubble residual bias to change with redshift and to be negative at low z and positive at high z. This is expected since NUV-red SNe, which should have their extinction overestimated and their distance moduli underestimated, are more prevalent in the local universe.

The magnitude of the bias depends on the magnitude of the $b - v$ difference. The first simulation, which uses the measured difference directly from the NUV subclasses, indicates a bias of HR $= 0.15 \pm 0.11$ (0.18 ± 0.14) between $z = 0$ and $z \approx 0.5$ ($z \approx 1$), while the second simulation finds HR $= 0.07 \pm 0.02$ (0.09 ± 0.03) for the same redshifts. Of course the second simulation has a more statistically significant bias because of the relatively smaller uncertainty for the $b - v$ difference. Of particular note is that, given the current uncertainties, the first simulation is consistent with zero bias for all redshifts.

To investigate the potential effect of two UV-optical color groups on the w parameter, we have modified the SNANA (v10.34; Kessler et al. 2009) *SNLC-SIM* routines to allow us to incorporate a filter-dependent bias in the rest-frame MLCS2k2 model (Jha et al. 2006a) of the SN. As the *Swift* u band is considerably bluer than Johnson U, and we cannot definitively determine the difference in mean absolute magnitude between the NUV-red and NUV-blue groups given the current sample size, we parameterize the difference by a single value—the difference in the rest-frame U-band magnitude between the NUV-red and NUV-blue groups. To reduce the number of independent parameters, we related the bias in Johnson B to Johnson U via $\Delta B = 0.4\Delta U$. We have elected to study the effect for a range of different values from 0.0 mag (no bias or NUV-red) to −0.4 mag (strong blue NUV bias) in increments of −0.1 mag. This range is large enough to encompass the true value of the difference in absolute magnitudes between the NUV-red and NUV-blue populations, and this method can be used to determine more accurate values for the cosmological bias as more NUV measurements from *Swift* become available.

We find no advantage in using the *SALT2* model over the MLCS2k2 model for these simulations. As *SALT2* is an observer-frame light curve fitter that employs spectral surfaces, in order to simulate two groups with rest-frame NUV

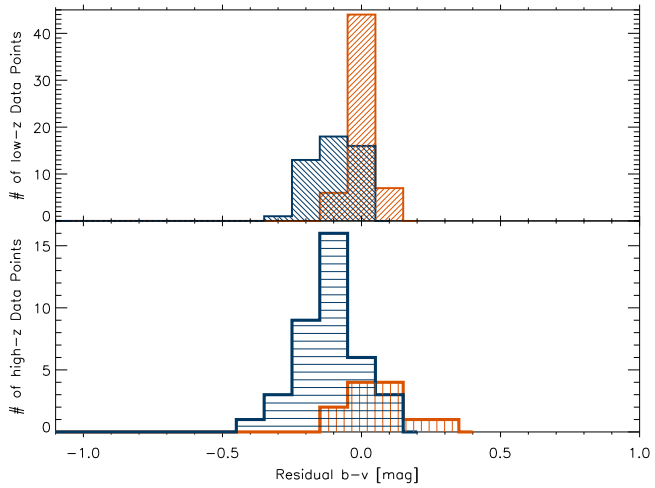

Figure 12. Histogram of residuals of low- & mid-z $b-v$ photometry vs. a quadratic fit to the UVOT NUV-red photometry. The upper panel shows UVOT NUV-red photometry (red) and UVOT NUV-blue photometry (blue). The lower panel shows mid-z spectrophotometry with NUV-red SNe Ia (red/vertical) and NUV-blue SNe Ia (blue/horizontal). The NUV-red/blue groups are not separated at either redshift, but the NUV-blue samples are bluer with overlap with the NUV-red samples. The low- and mid-z histograms peak at similar colors. Quadratic fit was for $|t - t_{\rm BPEAK}| \leqslant 10$ days.

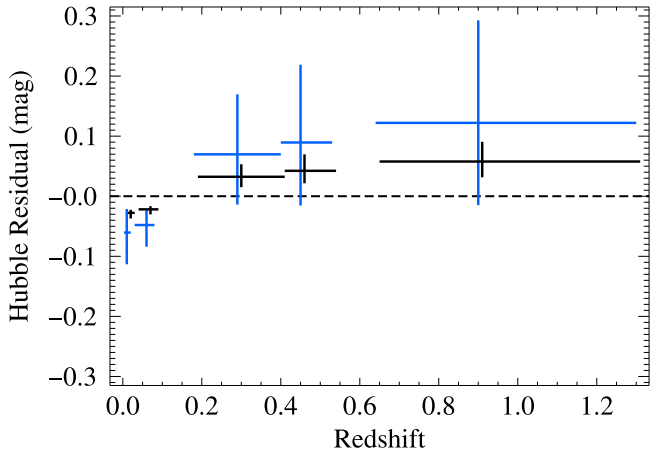

Figure 13. Simulated Hubble residuals due to the variations with redshift of the NUV-red/blue ratio and the HV/LV ratio. The solid blue points show Hubble Residuals based upon the observed $b-v$ color difference between NUV-red and NUV-blue SNe Ia. The solid black points show Hubble residuals based on the observed $b-v$ color difference between HV and LV SNe Ia, offset by 0.01 in redshift for display purposes. See text for details of the simulations.

differences we would have to warp the spectral surfaces with some color law in the rest-frame. This is equivalent to the MLCS2k2 treatment of excess color as reddening, as any cosmological bias is directly correlated with the specific form of the color law assumed to warp the spectral surfaces. Additionally, as we are differentially comparing low-z and high-z SNe, simulated using the same code, the addition of high redshift SNe in the *SALT2* training sample is not relevant. This difference between the two light curve fitting methodologies may prove significant if this study is conducted using real SNe Ia samples. However, given the significant extra systematics involved in combining different surveys, and our imprecise knowledge of the mean difference in absolute magnitudes of the two NUV groups, such a study is well beyond the scope of this paper.

We simulate 500 SNe Ia for each value of the bias, in a flat cosmology with $\Omega_M = 0.3$, $h_0 = 0.65$, and three different values of the dark energy equation of state, $w = -1, -0.5, 0$. Additional flux smearing is used to ensure the simulated light curves reproduce the observed scatter in the Hubble diagram, and the cosmological fits have reduced $\chi^2 \sim 1$. All SNe Ia are fit with MLCS2k2 with priors appropriate for the SNLS. The effect of the NUV bias on the MLCS2k2 fit parameters μ, A_V, and Δ are presented in Figure 14. MLCS2k2 interprets the excess blue color as reduced extinction, and the recovered A_V distribution becomes increasingly asymmetric and skewed to lower values with increase in the bias. However, as A_V is negatively correlated with the distance modulus, μ, increasing NUV bias leads to an increasing positive bias in the recovered distances. We find two effects with increasing redshift. As rest-frames I and R redshift out of the observer frame *griz* filters, the relative weight of U and B increases. Additionally, at very high-z, our simulation samples a very narrow range of low A_V, as we are unlikely to find heavily extincted SNe Ia. However, as MLCS2k2 does not allow negative A_V, this leads to a reduced bias in the recovered extinction at high-z. Consequently, the bias in recovered distance modulus first increases up to $z \approx 0.5$ and then decreases. The recovered light curve shape parameter, Δ, shows an increasing bias to more negative, or broader, intrinsically brighter models with increase in the strength of the NUV bias. Our simulation uses a simple magnitude offset as the bias, and does not alter light curve shape in any band, and we do not find any significant bias in the recovered time of maximum, as we would expect.

For each value of the bias, we create a combined sample of unbiased, NUV-red SNe Ia and NUV-blue SNe Ia consistent with Figure 4. We use the *simple-cosfitter*[10] (v1.6.11) package to estimate the cosmological parameters, Ω_M and w, for each combined sample, and compare the results to the cosmological parameters estimated from the full unbiased NUV-red sample. The effect of the NUV bias on the cosmological parameters is shown in Figure 15. As increasing the NUV bias leads to an increased positive bias in recovered distance modulus, μ, we find a bias toward more negative values of the equation of state parameter, w, from the SNe Ia data. When combined with the BAO prior, the joint constraints are biased toward lower values of w and higher values of O_M. However, the tension between our simulated SNe Ia data and the real BAO data also increases with increase in the bias. The 99.7% SNe Ia contours do not overlap with the the BAO contours in the case of the strong $\Delta U = -0.4$ mag bias, and the combined constraints are not meaningful. It is likely that biases over $\Delta U = 0.3$ mag are unphysical. The increased tension is not captured by the results from simple parameter marginalization shown in Figure 16.

There are several limitations in these simulations—given the small sample size presented in this work, there is still considerable uncertainty about the size of the difference between the NUV colors, the physical mechanism that causes it, and the relative ratio of the two groups and its evolution with redshift. Additionally, we have made several simplifying assumptions such as simulating a single survey and relating the bias in Johnson B to Johnson U. More extensive analysis would be premature given the current sample size. The quantitative results shown in Figure 16 can only be interpreted within the context of these limitations, and the qualitative

[10] http://qold.astro.utoronto.ca/conley/simple_cosfitter

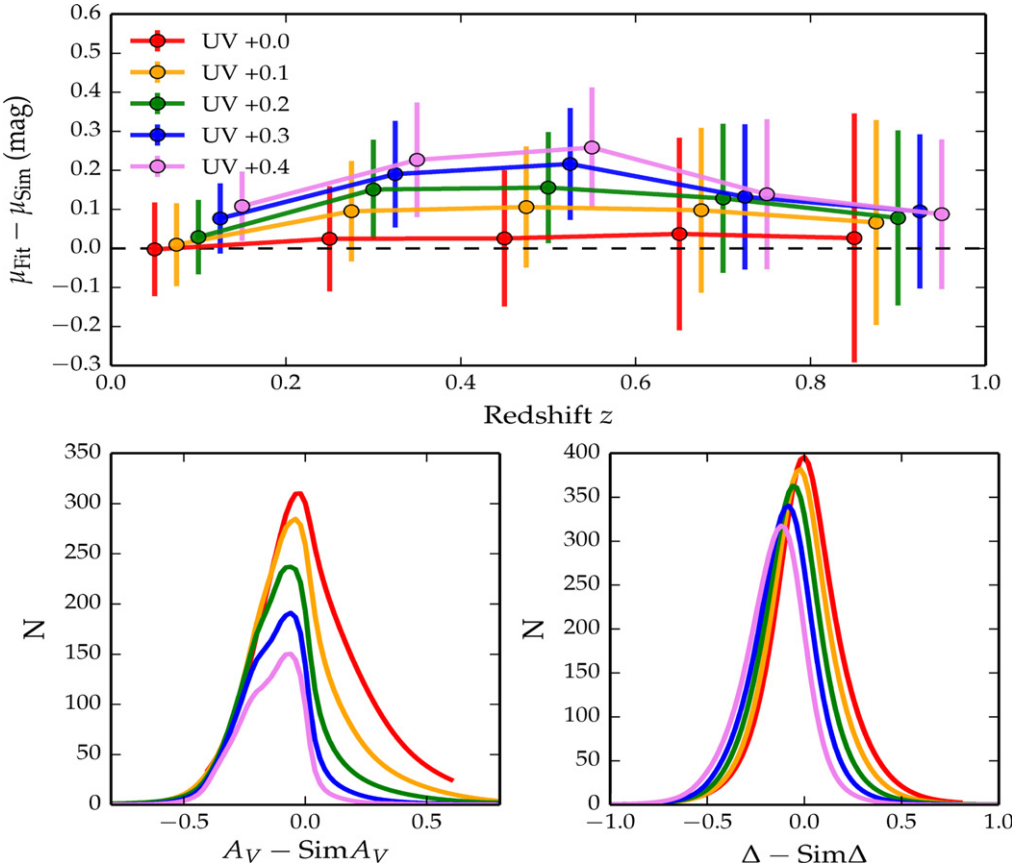

Figure 14. Differences between fit and simulated light curve parameters with bias increasing from $\Delta U = 0.0$ mag (red) to −0.40 mag (violet). Increasing the NUV bias causes MLCS2k2 to favor lower values of the extinction A_V and light curve shape parameter Δ (lower panels) in order to fit the brighter and bluer SNe Ia light curves. As the distance modulus, μ, is negatively correlated with A_V, the light curve fitter exhibits a systematic bias to higher distances. There is significant evolution of the mean distance modulus bias with redshift (upper panel, shown using the mean residual in redshift bins of 0.2, with different values of the bias offset slightly along the x-axis for clarity) arising from a combination of effects. The standard deviation of the residuals in each bin is shown in each bin, to indicate the range spanned by the data. Our simulated light curves are "flux smeared" to replicate the observed scatter in the Hubble diagram, with reasonable intrinsic dispersion.

behavior seen within light curve fit parameter residuals and the cosmological contours arguably offers more insight. In particular, the tension between our simulated SNe Ia data and the real BAO constraints is similar to the tension observed between constraints from *Planck* and the Union 2.1 supernova set (Rest et al. 2014). There are many sources of systematics or potential new physics that could cause the observed tension between the SNe Ia data and the results from CMB experiments, and we cannot definitively ascribe it to the effect of two groups of UV-optical colors in SNe Ia. As the size of the *Swift* SNe Ia sample increases, and high-z searches such as Pan-STARRS and DES probe the rest-frame UV with better S/N, it will become possible to identify and characterize different color groups more thoroughly.

Absolute magnitudes of the early UVOT SNe Ia were presented in Brown et al. (2010). That sample was dominated by NUV-red events with a single NUV-blue SN, 2008Q, and used existing color relations and extinction laws. Rather than extend that methodology to the current, larger sample, it is important to wait until an improved treatment of intrinsic colors and extinction is developed, and present the absolute magnitudes of the UVOT sample at that time. Efforts are also being made to observe SNe Ia in the nearby Hubble flow with UVOT to reduce the effect of peculiar and/or thermal velocities on the redshift-derived distances. For the more nearby SNe, improved distances using Cepheids or other distance indicators would allow the differences seen in the UV photometry, as well as spectroscopy (Foley & Kirshner 2013), to be compared directly to the absolute magnitudes in the optical.

6. SUMMARY

The existence of two UV-optical color groups among normal SNe Ia has been established by UVOT photometric observations. Three mid-z spectroscopic samples have had spectrophotometry performed to produce UVOT u, b, and v spectrophotometry. The three samples have been combined and compared with the UVOT low-z sample, finding the same two groups at higher redshift. The colors within each group match the low-z colors, but the bluer NUV-blue group dominates at high-z (90%), the opposite of what is seen at low-z (∼33%). This change appears to be the explanation for the difference between the high-z mean spectra and low-z mean spectra that were generated from these samples. A higher redshift sample exhibits an even stronger dominance of NUV-blue events.

Separating the mid-z sample into NUV-red/blue groups, we investigate the $u - b$ and $b - v$ colors. The $u - b$ colors also exhibit an NUV-red/blue separation, with the NUV-blue group again the bluer group, but the two samples begin to overlap. The $b - v$ color features significant overlap, but the NUV-blue sample is bluer on average by 0.1–0.2 mag. This presents problems for methods of extinction estimation for SNe Ia that

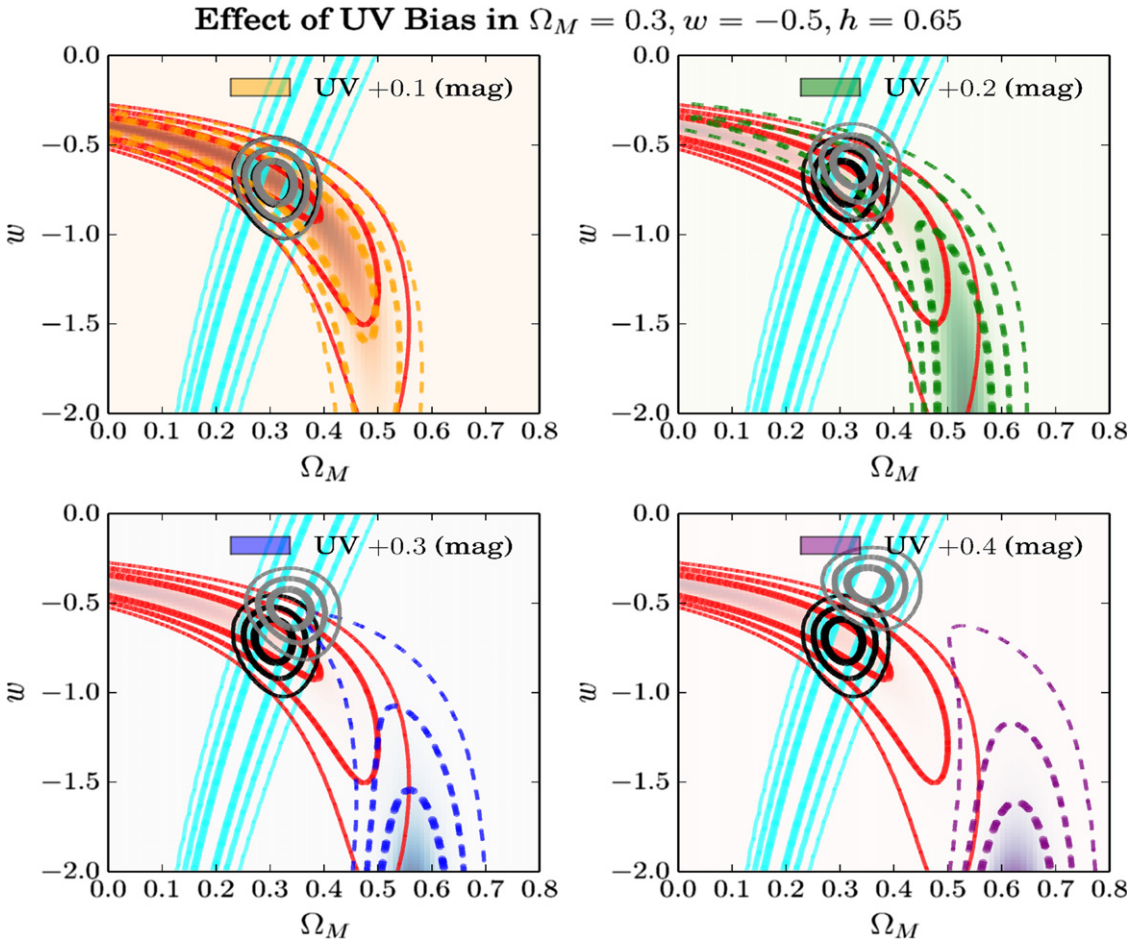

Figure 15. Effect of increasing NUV bias on cosmological inference in a flat $\Omega_M = 0.3$, $w = -1$, $h_0 = 0.65$ cosmology. The BAO contours are shown in cyan, while the unbiased, or NUV-red, sample is shown in red. The dashed contours show the effect of combining the NUV-blue and NUV-red SNe I for different values of the bias (colors correspond to those shown in the legend and Figure 14). As increased bias leads to systematically higher distance determinations, we find the SNe Ia contours are systematically biased to more negative values of the dark energy equation of state, w, and higher Ω_M. However, the combined BAO and SNe Ia constraints (shown in black for the NUV-red sample, and gray for the combined sample) are biased toward lower values of w, and there is a strong increase in the tension between the two data sets. These results indicate that values of the bias above $\Delta U = -0.3$ mag are implausible. The tension is qualitatively similar to the tension seen between the Union 2.1 supernova sample and the *Planck* constraints.

utilize $B - V$ colors, as existing methods do not differentiate NUV-red/blue events. The use of SNe Ia as cosmological distance indicators rely upon distant SNe Ia being similar to nearby SNe Ia, at least to the extent that there are nearby reference SNe Ia for all distant SNe Ia. The finding that NUV-blue events dominate distant SNe Ia means that the absolute magnitudes, and a separate luminosity-width relation, needs to be derived for this group of normal SNe Ia.

We found that the NUV color differences were highly correlated with the measured ejecta velocity. Optical color differences have also been reported between normal SNe Ia that have been divided into two groups based upon the blueshift of a prominent Si II λ6355 absorption feature (Foley & Kasen 2011; Foley et al. 2011, F12). Foley & Kasen (2011) suggested that the physical reason for the correlation between color and ejecta velocity was driven by the connection between the depth of the line-forming region within the ejecta and the opacity. One can interpret this connection as higher ejecta velocities causing overlapping lines and thus increased opacity and redder $B - V$ colors, or as increased Fe-group abundance increasing the opacity and causing the line-forming region for intermediate-mass elements to be farther out in the ejecta and thus at higher velocity.

M13 showed that NUV-blue SNe Ia have low velocities while the NUV-red SNe Ia are equally mixed between low- and high-velocity objects. Approximately two-thirds of low-z SNe Ia have LV ejecta (e.g., Foley et al. 2011). Meanwhile, about one-third of low-z SNe Ia are NUV-blue. Low-z SNe Ia can be separated into two roughly equal-sized groups: LV/NUV-blue, LV/NUV-red, and high-velocity/NUV-red. The LV/NUV-blue events are bluer in $B - V$, leading to the observed color differences.

This contrasts with the mid-z sample, where about three-quarters of the sample are NUV-blue. For the subsample in which we could determine their ejecta velocities, the mid-z NUV-blue SNe were essentially all LV, while half of the mid-z NUV-red SNe are high-velocity. Therefore, the three groups listed above, LV/NUV-blue, LV/NUV-red, and high-velocity/NUV-red, have approximate fractions of 76%, 12%, and 12%, respectively.

We note that these fractions are seen for a subsample of mid-z SNe Ia, specifically those with relatively high-quality spectra. As detailed by E08 and F12, it is unlikely that these subsamples had selection effects that caused this color difference. However, it is possible that the true fractions for the entire SN Ia

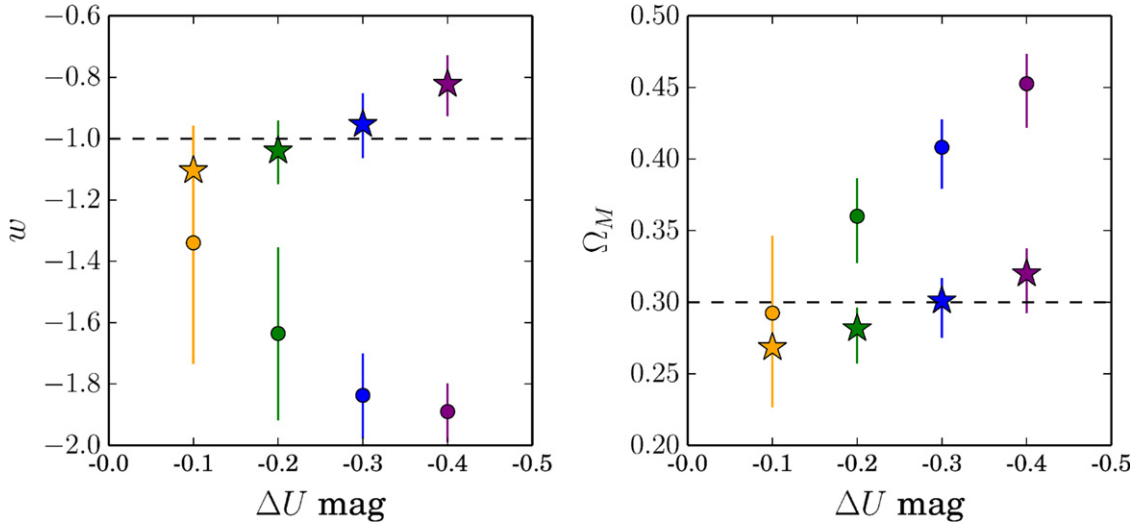

Figure 16. 1D marginalized values of Ω_M and w as a function of the bias for SNe Ia only (circles) and joint SNe Ia and BAO data sets (stars). There are clear trends illustrating that the cosmological parameter bias increases from the SNe Ia only as the NUV bias is increased. While the joint constraints appear superficially to show much less bias, this is illusory as the tension between the two data sets increases with bias two, as evidenced by the divergence of the two trends. The dark energy equation of state, w, is significantly more strongly impacted by increasing NUV bias. This is not unexpected as the BAO data alone are a strong constraint on Ω_M.

population at higher redshifts could vary from those reported here.

These findings motivate revisiting the SN templates that are used in comparisons with high-redshift SNe Ia. Two sets of templates should be produced, one for NUV-blue SNe Ia and one for NUV-red SNe Ia. A key qualification for inclusion into the new template sets will be whether NUV-red/blue membership can be determined. For archival SN Ia observations, that would require that at least some observations of a given SN were performed with a detector with acceptable blue sensitivity, to allow clear separation between NUV-red and NUV-blue. For future SN Ia observations, these findings suggest placing a high priority on detectors with excellent blue sensitivity, or building a template set from UVOT-observed SNe Ia. An alternative possibility would be for the observations of known NUV-red and NUV-blue SNe to reveal another observable characteristic that completely correlates with the NUV-optical. Along those same lines, it will be important to understand the associations between NUV-red/blue groupings and other characteristics that are independent of peak width, such as: HV/LV grouping, the presence or absence of unburned carbon in early epoch spectra, whether the late *B* and *V* band photometry follows the Lira relation, and whether the optical spectra show evidence of strong Na D absorption lines. Collectively, correlations between these groupings will be a powerful probe of the progenitor metallicity, the binary pair, and the explosion physics of the different varieties of SNe Ia.

P.A.M. acknowledges support from NASA ADAP grant NNX10AD58G. P.J.B. is supported by the Mitchell Postdoctoral Fellowship and NSF grant AST-0708873. All supernova observers thank the mission operations team at Penn State for scheduling the thousands of individual UVOT target-of-opportunity observations that comprise the UVOT dataset. The NASA/IPAC Extragalactic Database (NED) was utilized in this work. NED is operated by the Jet Propulsion Laboratory of the California Institute of Technology, under contract with the National Aeronautics and Space Administration.

REFERENCES

Arsenijevic, M., Fabbro, S., Mourao, A. M., & Rica da Silva, A. J. 2008, A&A, 492, 535
Balland, C., Baumont, S., Basa, S., et al. 2009, A&A, 507, 85
Baumont, S., Balland, C., Astier, P., et al. 2008, A&A, 491, 567
Blondin, S., Mandel., K. S., & Kirshner, R. P. 2011, A&A, 526, A81
Breeveld, A. A., Curran, P. A., Hoversten, E. A., et al. 2011, in AIP Conf. Proc. 1358, Gamma Ray Bursts 2010, ed. J. E. McEnery, J. L. Racusin, & N. Gehrels, 373
Brown, P. J., Dawson, K. S., de Pasquale, M., et al. 2012, ApJ, 753, 22
Brown, P. J., Kuin, P., Scalzo, R., et al. 2014, ApJ, 787, 29
Brown, P. J., Roming, P. W. A., Milne, P. A., et al. 2010, AJ, 721, 1608
Bufano, F., Immler, S., Turatto, M., et al. 2009, ApJ, 700, 1456
Childress, M. J., Filippenko, A. V., Ganeshalingam, M., & Schmidt, B. P. 2014, MNRAS, 437, 338
Conley, A., Sullivan, M., Hsiao, E. Y., et al. 2008, ApJ, 681, 482
Cooke, J., Ellis, R. S., Sullivan, M., et al. 2011, ApJ, 727, 35
Ellis, R. S., Sullivan, M., Nugent, P. E., et al. 2008, ApJ, 674, 51
Foley, R. J. 2012, ApJ, 748, 127
Foley, R. J., Brown, P. J., Rest, A., et al. 2010, ApJ, 708, 1748
Foley, R. J., Challis, P. J., Chornock, R., et al. 2013, ApJ, 767, 57
Foley, R. J., Challis, P. J., Filippenko, A. V., et al. 2012a, ApJ, 744, 38
Foley, R. J., Filippenko, A. V., Aguilera, C., et al. 2008, ApJ, 684, 68
Foley, R. J., Filippenko, A. V., Kessler, R., et al. 2012c, AJ, 143, 113
Foley, R. J., & Kasen, D. 2011, ApJ, 729, 55
Foley, R. J., Kromer, M., Marion, G. H., et al. 2012b, ApJL, 753, L5
Foley, R. J., & Kirshner, R. P. 2013, ApJL, 769, L1
Foley, R. J., Sanders, N. E., & Kirshner, R. P. 2011, ApJ, 742, 89
Folatelli, G., Phillips, M. M., Burns, C. R., et al. 2010, AJ, 139, 120
Folatelli, G., Phillips, M. M., Morrell, N., et al. 2012, ApJ, 745, 74
Guy, J., Sullivan, M., Conley, A., et al. 2010, A&A, 523, 7
Hachinger, S., Mazzali, P. A., Sullivan, M., et al. 2013, MNRAS, 429, 2228
Hicken, M., Garnavich, P. M., Prieto, J. L., et al. 2007, ApJL, 669, L17
Hicken, M., Wood-Vasey, W. M., Blondin, S., et al. 2009, ApJ, 700, 1097
Hőflich, P., Wheeler, J. C., & Thielemann, F. K. 1998, ApJ, 495, 617
Howell, D. A., Sullivan, M., Nugent, P. E., et al. 2006, Natur, 443, 308
Jha, S., Branch, D., Chornock, R., et al. 2006b, AJ, 132, 189
Jha, S., Kirshner, R. P., Challis, P., et al. 2006a, AJ, 131, 527
Jha, S., Riess, A., & Kirshner, R. P. 2007, ApJ, 659, 122
Kessler, R., Becker, A. C., Cinabro, D., et al. 2009, ApJS, 185, 32
Kirshner, R. P., Jeffery, D. J., Leibundgut, B., et al. 1993, ApJ, 415, 589
Krisciunas, K., Marion, G. H., Suntzeff, N. B., et al. 2009, AJ, 138, 1584

Lentz, E. J., Baron, E., Branch, D., Hauschildt, P. H., & Nugent, P. E. 2000, ApJ, 530, 966
Li, W., Filippenko, A. V., Gates, E., et al. 2001, PASP, 113, 1178
Li, W., Filippenko, A. V., Gates, E., et al. 2003, PASP, 115, 453
Lira, P. 1995, Masters thesis, Univ. Chile
Maguire, K., di Carlo, E., Smartt, S. J., et al. 2010, MNRAS, 418, 747
Maguire, K., Sullivan, M., Ellis, R. S., et al. 2012, MNRAS, 426, 2359
Mazzali, P. A., Sullivan, M., Hachinger, S., et al. 2014, MNRAS, 439, 1959
Milne, P. A., Brown, P. J., Roming, P. W. A., et al. 2010, AJ, 721, 1627
Milne, P. A., Brown, P. J., Roming, P. W. A., et al. 2013, ApJ, 779, 23
Nordin, J., Ostman, L., Goobar, A., et al. 2011, ApJ, 734, 42
Parrent, J., Thomas, R. C., Fesen, R. A., et al. 2011, ApJ, 732, 30
Perlmutter, S., Aldering, G., Goldhaber, G., et al. 1999, ApJ, 517, 565
Perlmutter, S., Gabi, S., Goldhaber, G., et al. 1997, ApJ, 483, 565
Phillips, M. M. 1993, ApJL, 413, L105
Phillips, M. M., Lira, P., Suntzeff, N. B., et al. 1999, AJ, 118, 1766
Poole, T., Breeveld, A. A., Page, M. J., et al. 2008, MNRAS, 383, 627
Rest, A., Scolnic, D., Foley, R. J., et al. 2014, ApJ, 795, 44
Riess, A. G., Filippenko, A. V., Challis, P., et al. 1998, AJ, 116, 1009
Riess, A. G., Press, W. H., & Kirshner, R. P. 1996, ApJ, 473, 88
Riess, A. G., Strolger, L.-G., Casertano, S., et al. 2007, ApJ, 659, 98
Roepke, F. K., Kromer, M., Seitenzahl, I. R., et al. 2012, ApJL, 750, L19
Roming, P. W. A., Kennedy, T. E., Mason, K. O., et al. 2005, SSRv, 120, 95
Sauer, D. N., Mazzali, P. A., Blondin, S., et al. 2008, MNRAS, 391, 1605
Scalzo, R., Aldering, G., Antilogus, P., et al. 2010, ApJ, 713, 1073
Silverman, J., & Filippenko, A. V. 2012, MNRAS, 425, 1917
Silverman, J., Ganeshalingam, M., Li, W., et al. 2011, MNRAS, 410, 585
Silverman, J. M., Ganeshalingam, M., Li, W., et al. 2011, MNRAS, 410, 585
Silverman, J., Kong, J. J., & Filippenko, A. V. 2011, MNRAS, 425, 1819
Sullivan, M., Ellis, R. S., Howell, D. A., et al. 2009, ApJ, 693, 76
Sullivan, M., Guy, J., Conley, A., et al. 2011, ApJ, 737, 102
Sullivan, M., Kasliwal, M. M., Nugent, P. E., et al. 2011, ApJ, 732, 118
Taubenberger, S., Hachinger, S., Pignata, G., et al. 2008, MNRAS, 385, 75
Thomas, R. C., Aldering, G., Antilogus, P., et al. 2011, ApJ, 743, 27
Timmes, F. X., Brown, E. F., Truran, J. W., et al. 2003, ApJ, 590, 82
Walker, E. S., Fabian, A. C., Sanders, J. S., et al. 2012, MNRAS, 427, 103
Wang, X., Filippenko, A. V., Ganeshalingam, M., et al. 2009b, ApJ, 699, 139
Wang, X., Li, W., Filippenko, A. V., et al. 2009a, ApJ, 697, 380
Wang, X., Wang, L., Filippenko, A. V., et al. 2012, ApJ, 749, 126
Yamanaka, M., Kawabata, K. S., Kinugasa, K., et al. 2009, ApJL, 707, L118